中国光学（中英文） Chinese Optics 核心期刊

基于半导体性单壁碳纳米管/富勒烯异质结的高性能透明全碳光电探测器

张罗茜 尹欢 陈越 朱明奎 苏言杰

High-performance transparent all-carbon photodetectors based on the semiconducting single-walled carbon nanotube/fullerene heterojunctions

ZHANG Luo-xi, YIN Huan, CHEN Yue, ZHU Ming-kui, SU Yan-jie

引用本文:
张罗茜, 尹欢, 陈越, 朱明奎, 苏言杰. 基于半导体性单壁碳纳米管/富勒烯异质结的高性能透明全碳光电探测器[J]. 中国光学, 2023, 16(5): 1243-1256. doi: 10.37188/CO.2022-0243
ZHANG Luo-xi, YIN Huan, CHEN Yue, ZHU Ming-kui, SU Yan-jie. High-performance transparent all-carbon photodetectors based on the semiconducting single-walled carbon nanotube/fullerene heterojunctions[J]. *Chinese Optics*, 2023, 16(5): 1243-1256. doi: 10.37188/CO.2022-0243

在线阅读 View online: https://doi.org/10.37188/CO.2022-0243

文章编号　2097-1842(2023)05-1243-14

High-performance transparent all-carbon photodetectors based on the semiconducting single-walled carbon nanotube/fullerene heterojunctions

ZHANG Luo-xi, YIN Huan, CHEN Yue, ZHU Ming-kui, SU Yan-jie*
(*Key Laboratory of Film and Microfabrication (Ministry of Education)*, *School of Electronics*, *Information and Electrical Engineering*, *Shanghai Jiao Tong University*, *Shanghai* 200240, *China*)
* *Corresponding author*, *E-mail*: *yanjiesu@sjtu.edu.cn*

Abstract: Taking advantage of the high absorption coefficient, excellent photoelectric properties, and high carrier mobility of Single-Walled Carbon NanoTubes (SWCNTs), high-performance, transparent, all-carbon Field-Effect Transistor (FET) photodetector has been constructed with a high transmittance more than 80% in the visible light band, in which semiconducting SWCNT (sc-SWCNT)/fullerene (C_{60}) heterojunctions as the channel materials, patterned metallic SWCNT film as source/drain electrodes, graphene oxide (GO) as the dielectric layer, and Indium Tin Oxide (ITO) as a transparent gate electrode. The electrical test results show that the photodetector exhibits a strong gate-tunable characteristics, and achieves a broadband spectral response from 405 to 1 064 nm in the visible-near infrared spectral region. Under 940 nm illumination with a light density of 5 mW/cm^2, the maximum photoelectric responsivity of 18.55 A/W and a specific detectivity of 5.35×10^{11} Jones can be achieved.

Key words: single-walled carbon nanotubes; Fullerene; all-carbon heterojunctions; high transparency; field-effect transistor photodetector

基于半导体性单壁碳纳米管/富勒烯异质结的高性能透明全碳光电探测器

张罗茜,尹　欢,陈　越,朱明奎,苏言杰*
(上海交通大学电子信息与电气工程学院 薄膜与微细技术教育部重点实验室,上海 200240)

摘要:利用半导体性单壁碳纳米管(SWCNT)的高吸收系数、优异的光电特性和高载流子迁移率等特点,本文构筑了基于半导体 SWCNT(sc-SWCNT)/富勒烯(C_{60})异质结的透明全碳宽光谱的场效应晶体管光电探测器。该器件的大部分结构均由碳基材料组成,全碳异质结作为导电沟道材料,金属性 SWCNT 作为源漏电极,氧化石墨烯(GO)作为介质层,在可见光波段的透光率均高于 80%。电学测试结果表明:该光电探测器表现出了较强的栅控能力,实现了从 405~

收稿日期:2022-11-24; **修订日期:**2022-12-12
基金项目:国家自然科学基金(No. 61974089)
Supported by the National Natural Science Foundation of China (No. 61974089)

1 064 nm 的可见光-近红外宽光谱响应，在 5 mW/cm^2 的 940 nm 激光照射下，该器件光电响应率可以达到 18.55 A/W，比探测率达到 5.35×10^{11} Jones，同时，表现出了优异的循环稳定性。

关 键 词：单壁碳纳米管；富勒烯；全碳异质结；高透明度；场效应晶体管光电探测器

中图分类号：TN15 **文献标志码：**A **doi:** 10.37188/CO.2022-0243

1 Introduction

Due to the rapid development of semiconductor technology and information science, the research on photosensitive devices has received extensive attention. Photosensitive devices play a crucial core role in modern optical detection, optical communication, optical information processing, and optical control technologies in industrial technology, national defense, military, and civilian fields. As the scale and diversity of applications are increasing, the demand for light detection devices with higher speed, high conversion efficiency or wide wavelength range, flexibility, and transparency is becoming more prominent. Moreover, there are increasing requirements for the operational performance of photodetectors, such as high sensitivity and responsivity as well as fast response speed, low noise and low power consumption of the devices in the operating wavelength band[1]. Kobe University[2] has developed an infrared sensor with high responsivity at RT, and the central part of the device is an $Al_{0.3}Ga_{0.7}As$/GaAs heterostructure. The maximum photoelectric responsivity of 0.8 A/W and a specific detectivity of 1.8×10^{10} Jones are achieved at about 6.6 μm at a bias of 1V. Although conventional silicon-based photodetectors have the advantages of mature preparation process and low cost, the wide band gap of silicon materials (≈1.12 eV) limits the range in working wavelength[3]. In addition, the energy band structure of the indirect band gap of silicon material makes it impossible to achieve high-efficiency photoelectric conversion, especially in the field of transparent optoelectronics. In this field, the light absorption capacity of materials such as silicon, germanium, indium gallium arsenic and other materials with high transparency is drastically reduced, making it difficult to achieve the perfect integration of high transparency and high optoelectronic performance. At present, most photoactive materials used in photodetectors are inorganic, and the manufacturing process of these materials requires high temperature and high energy consumption, and the growth process needs to use many complex methods. These methods are complex, sensitive to process fluctuations, and have high technical requirements. In addition, the processes and photoactive materials themselves typically contain harmful elements such as lead, mercury, cadmium and arsenic. Therefore, the development of NIR photodetectors based on new materials has gradually become a research focus in recent years.

Since the 1960s, the emerging field of organic electronics has made tremendous progress in catching up with inorganic semiconductor technology and now offers alternatives for many optoelectronic applications. The development of inorganic materials is currently dominated by inorganic semiconductors or metals, such as transparent electrodes, thin-film transistors, solar cells, and photodetectors. Among them, low-dimensional nanoscale materials have attracted much attention for their potential applications in new printable, highly integrated flexible and self-powered photochemical UV-NIR broad-spectrum photodetectors.

In recent years, allotrope structures of carbon such as fullerenes (C_{60}), carbon nanotubes, and graphene have attracted a great deal of research interest and experimental applications due to their superior chemical, physical, mechanical, and electronic properties. Depending on the chemical properties, some of these carbon materials are metallic and some are semiconducting and can form insulating oxides. Therefore, the use of these materials in combination to fabricate new optoelectronic devices

composed entirely of carbon-based materials offers some attractive possibilities for the development of next-generation electronic devices. Carbon-based materials are very abundant on Earth[3-4] and can be dispersed and deposited using solution processes, so they can be used directly in well-developed tools and processes[5], and these advantages lay the foundation for the development of carbon nanomaterials for research and applications. Due to their excellent electrical conductivity, high transparency and high robustness, carbon nanomaterials have received high attention, especially Single-Walled Carbon Nano Tubes (SWCNTs). As a typical quasi one-dimensional nanomaterial, SWCNTs have special electrical and optical properties[6-7] and have been extensively investigated in various application fields, such as transistors and solar cells[8-9]. According to their diameters and chirality, SWCNTs exhibit semiconducting or metallic characteristics[10]. The band gaps of semiconducting SWCNTs (sc-SWCNTs) with different diameters vary from 0.5 to 1.2 eV. Due to their ultra-high carrier mobility (10^5 cm^2/Vs), high absorption coefficients (10^4~10^5/cm), and long exciton diffusion length, sc-SWCNTs are commonly used as active materials for high-performance carbon-based photodetectors[11-12]. In addition, the electron transition of sc-SWCNTs is sensitive to polarized light due to their specific angular momentum in its subband gap, thus further expanding the detection applications of sc-SWCNTs-based photodetectors[13-14]. Due to the above unique properties, sc-SWCNTs have become an ideal material for light energy collection in broadband light detection.

There have been numerous reports on the research and applications of various photosensitive devices based on sc-SWCNTs. Researchers from Peking University[15] have developed an asymmetric structure based SWCNT photovoltaic type IR detector with a responsivity of 9.87×10^{-5} A /W and a detectivity of 10^7 Jones. This type of IR detector has the advantages of simple process and no cooling IR detection at RT. L Peng's team[16] also reported a high-performance photodiode based on carbon nanotubes treated by a dopant-free technique solution, which can operate at RT and zero bias. The broadband response range of the detector is 785 ~ 2 100 nm, and the detectivity exceeds 10^{11} Jones. However, the photogenerated electron/hole pairs in sc-SWCNTs usually remain in the exciton state, and the separation of excitons usually requires a strong electric field or an internal electric field to generate photocurrents in the external circuit. Therefore, the dissociation and transfer of excitons need to be enhanced by combining with other materials such as bulk semiconductors, nanomaterials, and polymers to form heterojunctions[17-19]. Due to its spherical structure, C_{60} has a high electron affinity and requires less recombination energy during electron transfer. Therefore, C_{60} tends to accelerate forward electron transfer and slow down reverse electron transfer, resulting in long-lived charge-separated states[20-22]. In various optoelectronic applications, C_{60} is commonly used as an efficient trapping material for photogenerated electrons, which generates higher photocurrents by trapping light-generated carriers and enabling longer carrier recombination lifetimes[23-24]. In addition, the all-carbon heterojunction constructed from sc-SWCNTs and C_{60} can also avoid interfacial atomic layer diffusion to a certain extent, which is more favorable for the dissociation of photogenerated electron-hole pairs[18]. A novel photodetector based on graphene nanoribbons-C_{60} heterostructures is prepared by Prof. Wang's group at Nanyang Technological University, Singapore. It can achieve a high photoresponsivity of 0.4 A/W under mid-infrared laser irradiation at room temperature, which enhanced the photoresponsivity of the transistor by about an order of magnitude over that of pure graphene[21]. This high performance is achieved by the high electron capture efficiency of the C_{60} film deposited on the graphene nanoribbon. Such carbon material heterojunction photodetectors pave the way for the realization of flexible and broadband photodetectors for various applications

such as imaging, remote sensing, and infrared camera sensors. On the other hand, field-effect transistors usually use gold as the electrode material, however, the use of gold will decrease optical transparency, while the use of metal-free devices such as SWCNT can not only achieve optical transparency and mechanical robustness, carbon-based conductive material also have advantages over other metal contacts in electrical contact carbon nanostructures.

Therefore, this paper constructs a transparent, all-carbon field-effect transistor-type photodetector based on sc-SWCNT/ C_{60} heterojunctions, metallic SWCNTs as source-drain electrodes, graphene oxide (GO) as the dielectric layer, and indium tin oxide (ITO) as the transparent gate. The high transmittance of the device was demonstrated by characterizing the light transmission of the sample by UV-Vis-NIR spectrophotometer. The modified sc-SWCNT material is characterized and analyzed by scanning electron microscopy and Raman spectroscopy for microscopic morphology and charge transfer level, and the results show that C_{60} played a p-type doping role for sc-SWCNT. The electrical tests demonstrate that the device has a more sensitive photoelectric response to visible-near-infrared light in the 405~1 064 nm band, expanding the application of the photodetector in next-generation transparent technologies such as smart windows and artificial intelligence glasses.

2 Experiment

2.1 Preparation of sc-SWCNT/ C_{60} all-carbon devices

First, the (6,5) SWCNT dispersion was prepared. 0.5 mg of (6,5) SWCNT powder (Sigma-Aldrich) was weighed and dispersed into 10 mL of aqueous sodium dodecyl sulfate (SDS) solution (0.01 g/mL). After 2 h of ultrasonic treatment in an ice bath, the inadequately dispersed (6,5) SWCNT powder was removed by centrifugation at 14 000 rpm for 30 min, and the supernatant after centrifugation was diluted 5 times to obtain a homogeneous (6,5) SWCNT dispersion. Then, GO films were prepared by vacuum extraction and filtration method and used as the dielectric layer of the transistors. After diluting the GO aqueous solution and sonicating at low temperature for 1 h, 10 mL of the dispersion was gradually added to a vacuum filtration device containing a 0.22 μm cellulose membrane and filtered to form a homogeneous GO film. After filtering the aqueous solution, excess deionized water was added to clean the excess SDS in the film 3 times to reduce its effect on the film performance. Finally, the GO films on the cellulose membranes were dried in a vacuum oven at 40 °C for 2 h. The aqueous graphene oxide solution was replaced with a homogeneous dispersion of metallic SWCNT in deionized water (0.05 mg/mL). Vacuum filtration was performed in the same way as described above to obtain uniform and dense conductive sc-SWCNT films as a backup material for the source-drain electrode.

ITO conductive glass with a thickness of 135 nm was used as the substrate and the gate electrode. First, the ITO conductive glass was cleaned with deionized water, acetone, isopropanol and ethanol in order to remove oil from the substrate surface. Then, the GO film on the prepared cellulose film was transferred to the ITO substrate, and the GO film was laminated and spread on the conductive glass surface using ethanol and water, and then the cellulose film was dissolved in acetone by soaking in acetone, and washed repeatedly with acetone to prevent the residual cellulose film on the substrate from affecting the device performance. Then, the above prepared sc-SWCNT dispersion was deposited on the GO surface by spin coating method at 2000 rpm to form a uniform film, and 2 mg of C_{60} was weighed by vacuum thermal evaporation method to make uniform vaporization onto the surface of the carbon tube film. The heterojunction of (6, 5) SWCNT/C_{60} on the substrate was constructed by annealing at 60 °C for 1 h under vacuum. Finally, the

metallic SWCNT film obtained by suction filtration was transferred to the sc-SWCNT/C_{60} heterojunction by repeating the above steps to form a source-drain pattern. The channel width between the source-drain electrodes is 200 μm and the length is 400 μm.

2.2　Testing and characterization

In this paper, the surface morphology of sc-SWCNT films/C_{60} heterojunctions as well as metallic SWCNT was characterized using a scanning electron microscope (SEM, Zeiss Ultra Plus, Germany). The transmission spectra were obtained by characterizing the transmittance of the samples to light using a Lambda 950 model UV-Vis-NIR spectrophotometer (USA). The Raman peak shifts of the heterojunction were analyzed by Raman spectroscopy statistics at an excitation wavelength of 514 nm. The optoelectronic properties of the devices were evaluated at room temperature using a semiconductor parameter analyzer, and the current-voltage (I-V) curves and current-time (I-T) curves of the devices were measured under the irradiation of various monochromatic laser diodes with adjustable power as the signal source of the optical pulses (laser wavelengths including 405, 532, 650, 780, 860, 940 and 1064nm).

3　Results and discussion

The structure diagram of the constructed field-effect transistor is shown in Figure 1(a), where ITO and GO form the gate and dielectric layer, sc-SWCNT/C_{60} heterojunction serves as the conductive channel, and metallic SWCNT forms the source-drain electrode. Figure 1(b) shows the optical transmission spectrum within the visible light range of the channel (sc-SWCNT/C_{60} film) region. The inset shows the physical image of the prepared field-effect transistor device. It is obvious that almost all carbon material films deposited on ITO are completely transparent, and their transmittance is only 10% lower than that of the substrate. When 80% of the substrate is covered with sc-SWCNT film (forming channels and electrodes), the optical transmittance of the device remains above 80%, indicating that the design of the device does not affect the light absorption of the channel layer itself. Figure 2(a) shows the carbon nanotubes deposited on GO by spin coating, sc-SWCNT is evenly distributed throughout the entire region, and no obvious surface dispersants or other polymers are visible in the image, demonstrating the high dispersibility of the nanotubes. The carbon tube solution dispersed and centrifuged by ultrasound ensures the uniformity and density of the sc-SWCNTs film. Figure 2(b) shows the SEM image of the sc-SWCNT/C_{60} composite film, from which it can be seen that C_{60} is uniformly distributed in the sc-SWCNT film. Figure 2(c) shows the SEM image of the metallic SWCNT as the source-drain electrode. It can be seen that a uniform and dense metallic SWCNT film was formed by suction filtration, which ensures good conductivity of the source-drain electrode.

Raman spectroscopy is the most used tool for

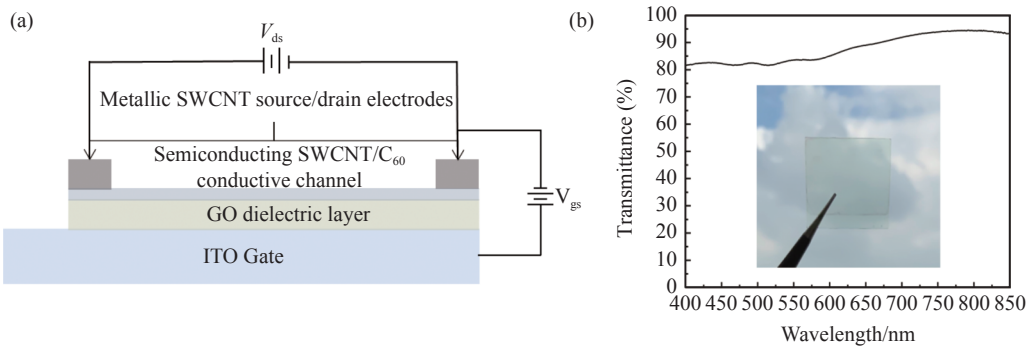

Fig. 1　(a) Schematic diagram of the device structure. (b) Transmittance of the device in visible band

图 1　(a) 器件结构示意图和 (b) 器件在可见光波段的透射率

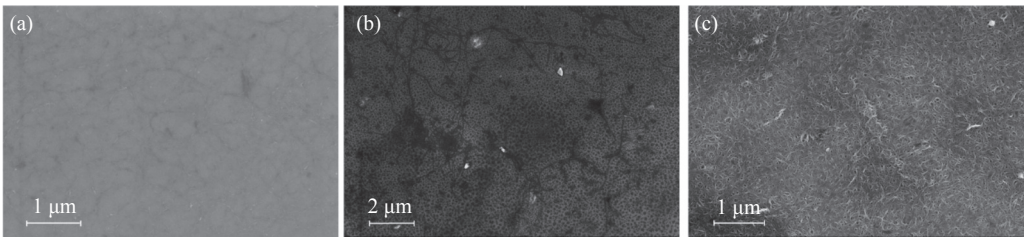

Fig. 2 Scanning electron microscope images of (a) sc-SWCNT film deposited by spin coating, (b) sc-SWCNT/C_{60} heterogeneous composite film and (c) m-SWCNT film

图 2 (a) 旋涂法沉积的 sc-SWCNT 薄膜、(b) sc-SWCNT/C_{60} 异质结复合薄膜和 (c) 金属性 SWCNT 薄膜的扫描电子显微镜图

studying carbon nanotubes. Raman spectroscopy can be used to analyze the doping effect of other materials on carbon nanotubes[25]. The change in doping level can be analyzed by observing the change in G and 2D peaks in Raman images. Figs. 3(a) and 3(b) (color online) show the Raman spectra of pristine and C_{60}-doped sc-SWCNT films in G and 2D modes. For sc-SWCNT, the D-peak in the 1 300~1 400 cm^{-1} region originates from the sp^3 defect in the carbon atom[26]. The strong tangential mode (G-peak) near 1 580 cm^{-1} arises from the in-plane vibrations of the sp^2 hybridized C=C bond in sc-SWCNT. sc-SWCNTs G-peaks consist of both G^+ (LO) and G^- (TO) modes[27], and the G^+ peaks represented by the analyzed LO phonons as well as the analog peaks of the 2D peaks are shown in light gray in the figure. After the addition of C_{60} to the sc-SWCNTs, a tendency to broaden and shift the two main peaks, G^+ and 2D, to higher energies is observed, and this change can be attributed to the doping effect of C_{60} on the sc-SWCNTs. It can be observed that the half-peak width of the G^+ peak of sc-SWCNT broadens from the original 20 cm^{-1} to 24 cm^{-1} after the addition of C_{60}. In addition, the peak position shifts to the right by 2.5 cm^{-1}, and the Raman spectrum of the 2D peak also produces a broadening of the half-peak width (about 4cm^{-1}) and a slight blue shift (from 2 634 cm^{-1} for pure sc-SWCNT to 2 636 cm^{-1} after C_{60} doping cm^{-1}) changes. These changes may be an indication of the p-type doping caused by C_{60} resulting in the transfer of electrons from the valence band of sc-SWCNT to C_{60}[28]. This suggests that there is a charge transfer between sc-SWCNT and the surrounding C_{60}, which causes p-type doping of (6,5)SWCNT.

The Raman analysis of sc-SWCNT/ C_{60} films described above has initially elucidated the charge transfer mechanism of the heterojunction channel of

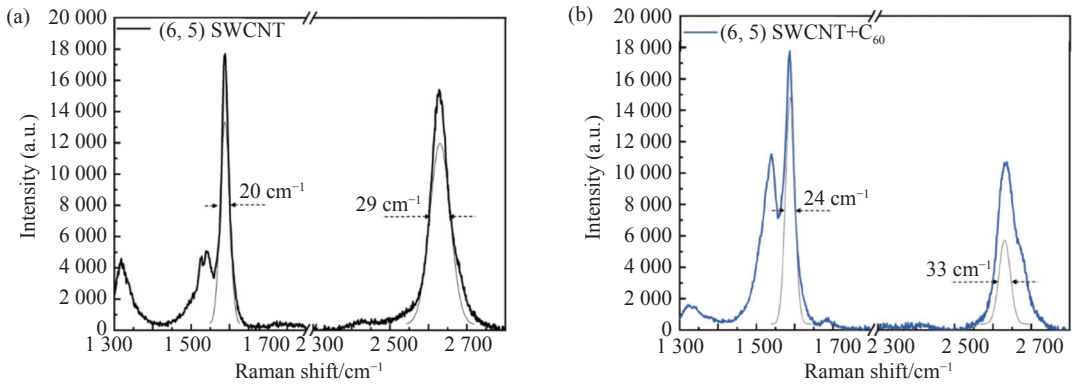

Fig. 3 Raman statistical analysis of sc-SWCNT /C_{60} film. Raman spectra of (a) sc-SWCNT (black) and (b) sc-SWCNT /C_{60} (blue) under 514 nm laser irradiation

图 3 sc-SWCNT/C_{60} 薄膜的拉曼统计分析。在 514 nm 激光辐照下 (a) sc-SWCNT (黑色) 和 (b) sc-SWCNT/C_{60} (蓝色) 的拉曼光谱

the prepared field-effect transistor and the operating mechanism. First, excitons are generated when the sc-SWCNTs are irradiated under light. Since the Lowest Unoccupied Molecular Orbit (LUMO) of C_{60} is lower than the conduction band of the sc-SWCNT, the photoexcited electrons of C_{60} cannot be transferred to the conduction band of the sc-SWCNT[29]. In addition, since the offset energy difference between $LUMO_{C60}$ and sc-SWCNT conduction band is greater than the exciton binding energy generated, electrons in the valence band of sc-SWCNT can be transferred into the Highest Occupied Molecular Orbital (HOMO) of C_{60}[30], producing charge separation, i.e., the transfer of photo-generated electrons from sc-SWCNT to the surrounding C_{60}, while the hole in sc-SWCNT density increases. As a result, the photogenerated excitons in the sc-SWCNT are effectively dissociated due to the structure of the designed heterojunction, reducing the recombination rate of photogenerated excitons[31-32]. This effective exciton collection allows the device to exhibit excellent optoelectronic properties.

The electrical performance of this heterojunction device is shown in Figure 4. With a constant source-drain voltage (V_{ds}) (V_{ds} = 0.1 V), the source-drain current (I_{ds}) can be changed by adjusting the carrier concentration in the channel by changing the gate voltage (V_{gs}), resulting in a transfer characteristic curve, as shown in Fig. 4(a). As can be seen from the figure, the turning point of the characteristic curve is about V_{gs}=1 V, indicating that the channel material sc-SWCNTs used during this period are p-type doped. When the applied gate pressure is less than the turning point, i.e., V_{gs} is on the left, more and more holes are induced in the channel as the absolute value of the gate pressure increases. As a majority carrier, the source-drain current of the device increases rapidly. On the contrary, the closer the gate voltage is to the turning point, the lower the concentration of holes in the channel, and the source-drain current decreases until the device shuts down. However, because the channel material is p-doped, the device cannot be completely shut down and there will still be an off-current of about 0.5 nA. When the gate voltage increases again above the turning point, electrons are induced in the channel, and the electron concentration increases with the further increase of the gate pressure, gradually replacing the hole to become the majority carrier, and gradually increasing the source-drain current in the opposite direction. The transconductance of the device is calculated to be 2.268×10^{-8} S, with a switching ratio of up to 500. The output characteristic curve of the device is obtained by linearly scanning the source-drain voltage V_{ds} from −1 V to 1 V while remaining the gate voltage V_{gs} constant. A cluster of output characteristic curves is obtained by testing the output characteristics for a range of V_{gs} values, as shown in Figure 4(b) (color online). It can be seen that the source-drain current shows a clear separation at different gate voltages, indicating that the device has a strong gate control capability. Besides, the device is bridged between source and drain electrodes by sc-SWCNT/C_{60} composite film, and the special electrical and optical properties of the all-carbon heterojunction provide a material basis for high-performance wide spectrum photodetection. Therefore, in this paper, the optoelectronic properties of the devices were investigated in room temperature air, as shown in Figs. 5(a) and 5(b) (color online). In addition, the I-V curves of the heterojunction devices under laser irradiation at different wavelengths and the I-T curves under unbiased voltage are shown, respectively. In order to test the photoelectric performance of the device, the source-drain current under a linear sweep of the bias voltage V_{ds} from -1 V to 1 V was tested using a semiconductor parametric analyzer at 405, 532, 650, 780, 860, 940, and 1 064 nm wavelengths (all laser powers were 5 mW/cm^2), respectively. We observed that at a bias voltage of 1 V, an induced photocurrent of about 0.7 μA can be generated. When the laser is repeatedly turned on and off, the photocurrent increases and decreases sharply respectively,

that is, the photodetector can show good repeated switching performance between switching states, indicating that the device has excellent reliability and cycle stability. In addition, the device exhibits significant optical response in the laser wavelength range of 405−1 064 nm, proving its wide spectral photoelectric response from visible light to near-infrared, and demonstrating certain advantages in the near-infrared band. In order to further evaluate the photoelectric performance of the heterojunction device, the responsivity and detectivity under different wavelength laser irradiation were calculated based on the measured photocurrent. The responsivity is defined as the photocurrent generated per unit area per unit illumination laser power density. The calculation formula is $R = \frac{I_p - I_d}{P \times A}$, where I_p is the induced photocurrent, I_d is the dark current without laser irradiation, P is the optical power density, and A is the area of the effective channel area of the device. The detectivity is generally used as an indicator of the detector's performance to detect the minimum optical signal, which can be used to evaluate the sensitivity of the device. The corresponding calculation formula is $D^* = \sqrt{\frac{A}{2qI_d}}R$, where q is the elementary charge, R is light responsiveness. It is calculated that the device can achieve the responsivity of 18.65 A/W and the detectivity of 5.35×10^{11} Jones under 940 nm laser irradiation at a power density of

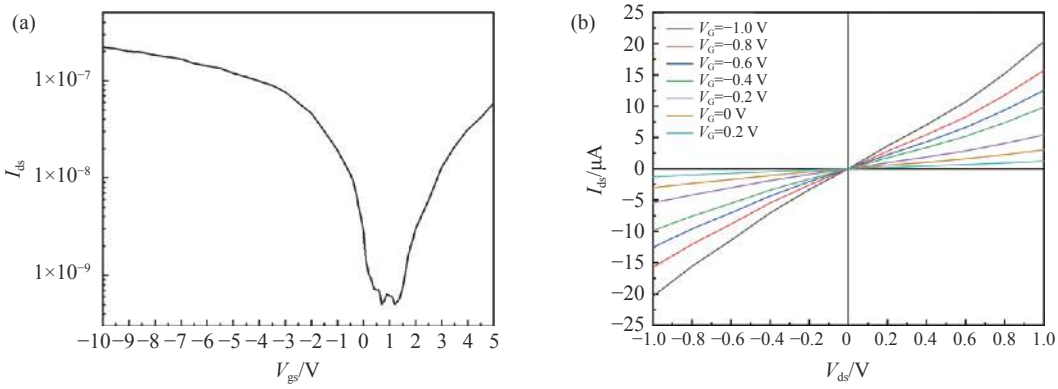

Fig. 4 (a) I_{ds}-V_{gs} curve and (b) I_{ds}-V_{ds} curve of the all-carbon device

图 4 全碳器件的 (a)I_{ds}-V_{gs} 曲线和 (b)I_{ds}-V_{ds} 曲线

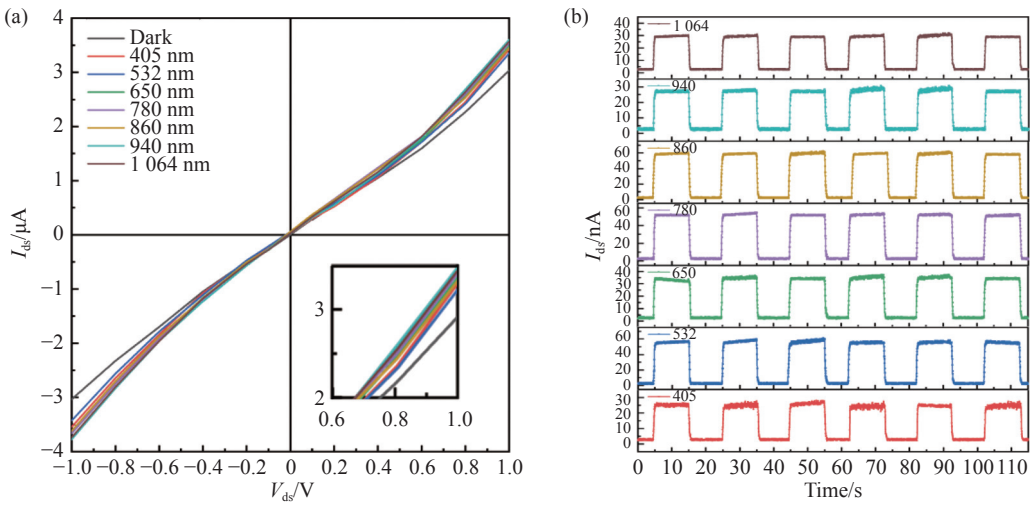

Fig. 5 (a) I_{ds}-V_{ds} curve and (b) I_{ds}-T curve of the all-carbon device under 405, 514, 650, 780, 860, 940, 1 064 nm laser irradiation

图 5 全碳异质结器件在不同波长(405, 514, 650, 780, 860, 940, 1 064 nm)激光照射下的 (a) I_{ds}-V_{ds} 和 (b) I_{ds}-T 曲线

5 mW/cm^2. The good photoelectric response performance is due to the ultra-high carrier mobility of sc-SWCNT, excellent optical absorption coefficient, long exciton diffusion length, and effective dissociation of excitons by C_{60} and transfer collection.

4 Conclusion

Taking advantage of the unique electronic properties and high carrier mobility of sc-SWCNT, a transparent, all-carbon field-effect transistor-type photodetector is designed and prepared in this paper. The components of this field-effect transistor (active channel, source-drain electrode, and dielectric layer) are all composed of carbon-based materials, and the transmittance of visible wavelengths are all higher than 80%. In addition to the large absorption coefficients and high conduction paths provided by the sc-SWCNTs, the proper energy band alignment between the sc-SWCNT and C_{60} interface and the separation of the photogenerated electron-hole pairs also lead to a significant enhancement of the photoelectric response performance of the device. Through the electrical test of the device, it has been proven that the device has good control ability over gate voltage. The responsivity and detectivity at 940 nm can reach 18.65 A/W and 5.35×10^{11} Jones, respectively, and a broad spectral response from 405 to 1 064 nm can be achieved, demonstrating the great advantage of sc-SWCNT/ C_{60} film heterojunctions for photodetectors. The results presented in this paper provide a new idea for the design and preparation of high-performance all-carbon-based optoelectronic devices, and provide a strong support for the development of next-generation of all-carbon transparent optoelectronic technology.

——中文对照版——

1 引 言

由于半导体技术和信息科学的快速发展，光敏器件的研究得到广泛关注和重视。光敏器件在现代光探测、光通信、光信息处理和光控制等工业技术、国防军事和民用光电技术领域起着关键作用。随着应用领域的规模和多样性的增长，对具有更高速度、更快转化效率或更宽波长范围以及高灵活性、高透明度的光检测器件的需求正变得越来越强烈。此外，对光电探测器的工作性能也提出越来越高的要求，如在工作波段下器件要有高灵敏度、高响应度且要具有快速响应和低噪声、低功耗等性能[1]。神户大学的学者[2]研发了在室温下具有高响应性的红外传感器，装置的中心部分是一个 $Al_{0.3}Ga_{0.7}As/GaAs$ 异质结构，在 1 V 偏置下，在约 6.6 μm 处的最大值为 0.8 A/W，比探测度为 1.8×10^{10} Jones。传统硅基光电探测器虽然具有制备工艺成熟、成本低等优势，然而硅材料较宽的带隙(≈1.12 eV)限制了其光电工作的波长范围[3]，另外，硅材料间接带隙的能带结构使得它无法实现高效率的光电转换。特别是在透明光电子领域，透明度较高的硅、锗、铟镓砷等材料的吸光能力大幅度下降，难以实现高透明度和高光电性能的完美融合。目前，大多数光电探测器所使用的光活性材料都是无机的，这些材料的制造需要经过几百摄氏度的高温、高能耗过程，生长过程中需要很多复杂方法。这些方法工艺复杂，对工艺的波动敏感，并且具有很高的技术要求。此外，工艺过程和光活性材料本身通常含有铅、汞、镉和砷等有害元素。因此，开发基于新材料的近红外光电探测器逐渐成为近年来的研究重点。

自 19 世纪 60 年代以来，新兴的有机电子领域取得了巨大的发展，不断追赶无机半导体技术，如今已经为许多光电应用提供了替代方案。无机材料目前主要以无机半导体或金属为主，如构成透明电极、薄膜晶体管、太阳能电池以及光电探测器等。其中，低维纳米级材料因其在新型可印刷、高集成度柔性和自供电光电化学紫外-近红外宽光谱光电探测器中的潜在应用而受到广泛关注。

近年来，富勒烯(C_{60})、碳纳米管、石墨烯等碳的同素异形体结构因其优越的化学、物理、机

械和电子性能吸引了大量研究人员的兴趣，进行了大量实验应用。由于化学性质的不同，这些碳材料有些是金属性的，有一些是半导体性的，并且可以组成绝缘的氧化物。因此，通过这些材料组合使用来制造完全由碳基材料组成的新型光电器件为下一代电子器件的发展提供了一些有吸引力的可能性。碳基材料在地球上的含量非常丰富[3-4]，并且可以使用溶液工艺进行分散和沉积，因此它们可以直接用于已成熟的工具和工艺中[5]。这些优势为碳纳米材料的研究和应用奠定了基础。碳纳米材料由于具有优异的导电性、高透明度和高鲁棒性而受到高度关注。单壁碳纳米管（SWCNT）作为典型的准一维纳米材料，具有特殊的电学和光学特性[6-7]，已经在多种应用领域中得到了广泛的研究，如晶体管、太阳能电池等[8-9]。根据其直径和手性的不同，SWCNT 表现出半导体或金属的特征[10]。不同直径的半导体性 SWCNTs（sc-SWCNTs）的带隙不同，从 0.5 到 1.2 eV 不等。由于 sc-SWCNTs 具有超高的载流子迁移率（10^5 cm^2/Vs）、高吸收系数（10^4~10^5/cm）和较长的激子扩散长度，使得 sc-SWCNTs 被普遍用于高性能碳基光电探测器的活性材料[11-12]。此外，由于 sc-SWCNTs 子带隙中的特定角动量，其电子跃迁对偏振光敏感，这进一步提升了基于 sc-SWCNTs 的光电探测器的检测应用[13-14]。由于上述独特的特性，sc-SWCNTs 已经成为宽带光探测中用于光能收集的理想材料。

基于 sc-SWCNTs 的各种光敏器件的研究和应用已有大量的报道。北京大学[15] 开发了一种基于非对称结构的 SWCNT 光伏型红外探测器，该探测器的响应率为 9.87×10^{-5} A/W，探测率为 10^7 Jones。这种类型的红外探测器具有工艺简单和室温下的无需冷却红外探测的优势。彭练矛团队[16] 还报道了一种通过无掺杂技术溶液处理碳纳米管基的高性能光电二极管，该二极管可以在室温和零偏压条件下工作。探测器的宽带响应范围为 785 ~ 2 100 nm，探测率超过 10^{11} Jones。然而，sc-SWCNTs 中的光生电子/空穴对通常保持在激子状态，激子的分离通常需要强电场或内部电场，才能在外部电路中产生光电流。因此，需要通过与其他材料（如体半导体、纳米材料和聚合物）结合形成异质结来增强激子的解离和转移[17-19]。由于为球形结构，C_{60} 在电子转移过程中具有较高的电子亲和度，需要较少的重组能量。因此，C_{60} 倾向于加速正向电子转移，减缓反向电子转移，从而形成长寿命的电荷分离态[20-22]。在各种光电子应用中，C_{60} 被普遍用作光致电子的高效捕获材料，该材料通过捕获光产生的载流子，使载流子重组寿命延长，从而产生更高的光电流[23-24]。另外，由 sc-SWCNTs 和 C_{60} 构筑的全碳异质结还可以一定程度上避免界面间的原子层扩散，更有利于光致电子空穴对的解离[18]。新加坡南洋理工大学王岐捷教授团队制备了一种基于石墨烯纳米带-C_{60} 杂化纳米结构的新型光电探测器，在室温下，在中红外激光照射下能够实现 0.4 A/W 的高光响应率，比纯石墨烯的晶体管光响应增强了约一个数量级[21]。这种高性能就是通过沉积在石墨烯纳米带上的 C_{60} 薄膜的高电子捕获效率实现的。这种碳材料异质结光电探测器为实现柔性和宽带光电探测器的各种应用铺平了道路，如成像，遥感和红外相机传感器。另一方面，场效应晶体管通常使用金作为电极材料，但是金的使用降低了光学透明度，采用 SWCNT 等无金属器件不仅可以实现光学透明度和机械鲁棒性，碳基导电材料在电接触碳纳米结构方面也比其他金属触点更有优势。

因此，本论文利用碳纳米材料独特的性能，基于 sc-SWCNT/C_{60} 异质结，以金属性 SWCNT 作为源漏电极，以氧化石墨烯（GO）作为介电层，氧化铟锡（ITO）作为透明栅极，构筑了一种透明、全碳场效应晶体管型光电探测器。通过紫外-可见-近红外分光光度计表征了样品对光的透过率，证明了器件具有很高的透光率。通过扫描电子显微镜及 Raman 光谱仪对修饰后的 sc-SWCNT 材料进行微观形貌和电荷转移水平的表征和分析，结果表明 C_{60} 对 sc-SWCNT 起到了 p 型掺杂的作用。通过电学测试证明了器件对 405~1 064 nm 波段的可见-近红外光具有较为灵敏的光电响应，拓展了光电探测器在智能窗、人工智能眼镜等下一代透明技术中的应用。

2 实验

2.1 sc-SWCNT/ C_{60} 全碳器件的制备

首先，制备 (6,5)SWCNT 分散液。称取 0.5 mg (6,5) SWCNT 粉末（Sigma-Aldrich）分散到 10 mL 十二烷基硫酸钠（SDS）水溶液（0.01 g/mL）中。冰

浴超声处理 2 h 后，以 14 000 rpm 离心 30 min，去除分散不充分的 (6,5) SWCNT 粉末，将离心后的上清液稀释 5 倍，得到均匀的 (6,5) SWCNT 分散液。其次，通过真空抽取和过滤法制备 GO 薄膜作为晶体管的介质层，将 GO 水溶液稀释并低温超声处理 1h 后，将 10 mL 分散液逐渐加入含有 0.22 μm 纤维素膜的真空过滤装置中过滤，形成均匀的 GO 薄膜，水溶液过滤后，加入过量的的去离子水清洗薄膜中多余的 SDS 3 次，以减少其对薄膜性能的影响。最后，将纤维素膜上的 GO 薄膜在 40 °C 真空烘箱中干燥 2 h。将氧化石墨烯水溶液替换为金属性 SWCNT 在去离子水中的均匀分散液（0.05 mg/mL）。用上述同样的方法，真空抽滤得到均匀致密的导电 sc-SWCNT 薄膜作为源漏电极的备用材料。

采用 135 nm 厚的 ITO 导电玻璃作为基底以及栅电极，首先，用去离子水、丙酮、异丙醇和乙醇依次清洗 ITO 导电玻璃，去除基底表面油污。然后，将制备好的纤维素膜上的 GO 薄膜转移到 ITO 基底上，利用乙醇和水将 GO 薄膜贴合铺展在导电玻璃表面，然后通过丙酮浸泡使纤维素膜溶解在丙酮中，并用丙酮反复清洗避免纤维素膜残留在基底上影响器件性能。之后，通过旋涂法将上述制备好的 sc-SWCNT 分散液以 2 000 rpm 的转速沉积在 GO 表面形成一层均匀的薄膜，并且通过真空热蒸发法称取 2mg C_{60} 使之均匀蒸镀到碳管薄膜表面，真空 60 °C 退火处理 1 小时，完成衬底上 (6, 5)SWCNT/ C_{60} 异质结的构筑。最后，将抽滤得到的金属性 SWCNT 薄膜通过重复上述步骤转移到 sc-SWCNT/C_{60} 异质结上，形成源漏电极图案，源漏电极之间的沟道宽度为 200 μm，长度为 400 μm。

2.2　测试与表征

本文使用扫描电子显微镜（SEM，德国蔡司 Ultra Plus）对 sc-SWCNT 薄膜/C_{60} 异质结以及金属性 SWCNT 的表面形貌进行了表征。用 Lambda 950 型号的紫外-可见-近红外分光光度计（美国）表征样品对光的透过率，得到透射光谱。在激发波长为 514 nm 的条件下，通过拉曼光谱统计对异质结的拉曼峰位移进行分析。利用半导体参数分析仪在室温下对器件的光电性能进行评价，并在由功率可调的多种单色激光二极管作为光脉冲信号源（激光波长包括 405, 532, 650, 780, 860, 940 和 1 064 nm）的照射下测量了器件的电流-电压（I-V）曲线和电流-时间（I-T）曲线。

3　结果与讨论

构筑的场效应晶体管结构图如图 1(a) 所示，其中 ITO 和 GO 构成栅极和介质层，sc-SWCNT/C_{60} 异质结作为导电沟道，金属性 SWCNT 构成源漏电极。如图 1(b) 显示了沟道（sc-SWCNT/C_{60} 薄膜）区域可见光范围内的光学透射光谱，其中插图为制备好的场效应晶体管的器件实物图。可以明显看出，ITO 上沉积的所有碳材料薄膜几乎都是完全透明的，其透过率仅仅比衬底低 10%，当 80% 的衬底均覆盖 sc-SWCNT 薄膜（形成沟道和电极）时，该器件的光学透过率依然保持在 80% 以上，说明器件的设计并不影响沟道层自身的光吸收。图 2(a) 展示了通过旋涂法在 GO 上沉积的碳管，sc-SWCNT 在整个区域均匀分布，并且在图像中看不到明显的表面分散剂以及其他聚合物。这证明纳米管具有较高的分散性，超声分散和离心的碳管溶液保证了 sc-SWCNTs 薄膜的均匀性和致密性。图 2(b) 是 sc-SWCNT/C_{60} 复合薄膜的 SEM 图像，从图中可以看到，C_{60} 均匀分布在 sc-SWCNT 薄膜中。图 2(c) 展示了作为源漏电极的金属性 SWCNT 的 SEM 图像，可以看出，通过抽滤法形成了均匀致密的金属性 SWCNT 薄膜，可以保证源漏电极具有良好的导电性。

拉曼光谱是研究碳纳米管最常用的工具，可以使用拉曼光谱来分析其他材料对碳纳米管的掺杂效应[25]。通过观察拉曼图像中 G 峰和 2D 峰的变化，可以分析掺杂水平的变化。图 3(a) 和 3(b) 为在 G 和 2D 模式下原始和 C_{60} 掺杂的 sc-SWCNT 薄膜的拉曼光谱。对于 sc-SWCNT，1 300~1 400 cm^{-1} 区域的 D 峰源于碳原子中的 sp^3 缺陷[26]。在 1 580 cm^{-1} 附近的强切向模（G 峰）则产生于 sc-SWCNT 中 sp^2 杂化 C=C 键的面内振动。Sc-SWCNTs 的 G 峰由 G^+（LO）和 G^-（TO）两种模式组成[27]，所分析的 LO 声子代表的 G^+峰以及 2D 峰的模拟峰在图中显示为浅灰色。在 sc-SWCNTs 中加入 C_{60} 后，观察到 G^+和 2D 两种主要峰的增宽和向能量更高的方向转移的趋势，这种变化可以归因于 C_{60} 对 sc-SWCNT 的掺杂效应。可以观

察到，加入 C_{60} 后，sc-SWCNT 的 G^+峰半峰宽从原来的 20 cm^{-1} 增宽到 24 cm^{-1}，此外，峰位置向右移动了 2.5 cm^{-1}，2D 峰的拉曼光谱也产生了半峰宽增宽（约 4cm^{-1}）和轻微的蓝移（从纯 sc-SWCNT 的 2634 cm^{-1} 到 C_{60} 掺杂后的 2636 cm^{-1}）。这些变化可能是由 C_{60} 引起的 p 型掺杂导致电子从 sc-SWCNT 的价带转移到 C_{60} 的迹象[28]。这表明，sc-SWCNT 与周围 C_{60} 之间存在电荷转移，C_{60} 对 (6,5) SWCNT 造成了 p 型掺杂。

通过上述对 sc-SWCNT /C_{60} 薄膜的拉曼分析，初步阐明了本文制备的场效应晶体管的异质结沟道的电荷转移机制以及工作机理。首先，当 sc-SWCNTs 在光照下照射时会产生激子。由于 C_{60} 的最低位占据分子轨道（LUMO）低于 sc-SWCNT 的导带，所以 C_{60} 的光激发电子不能转移到 sc-SWCNT 的导带[29]，又由于 $LUMO_{C60}$ 与 sc-SWCNT 导带之间的偏移能量差，大于产生的激子结合能，因此 sc-SWCNT 价带的电子可以转移到 C_{60} 最高占据分子轨道（HOMO）中[30]，产生电荷分离，即光生电子从 sc-SWCNT 转移到周围的 C_{60}，sc-SWCNT 中空穴的密度同时增加。因此，由于所设计的异质结结构，sc-SWCNT 中的光生激子被有效地解离，降低了光生激子的重组率[31-32]。这种有效的激子收集使该器件表现出卓越的光电特性。

该异质结器件的电学性能如图 4 所示。在源漏电压（V_{ds}）不变（V_{ds} = 0.1 V）的情况下，通过改变栅压（V_{gs}）调节沟道中的载流子浓度，从而改变源漏电流（I_{ds}），得到转移特性曲线，如图 4(a) 所示。从图中可以看出，特性曲线的转折点约在 V_{gs} = 1 V 左右，表明期间使用的沟道材料 sc-SWCNTs 是 p 型掺杂，当施加的栅压小于转折点，即 V_{gs} 位于左侧时，随着栅压绝对值的增大，沟道中感应出越来越多的空穴。作为多数载流子，器件的源漏电流快速增大，相反，栅极电压越接近转折点，沟道中的空穴浓度就越低，源漏电流减少直至器件关断，但是由于沟道材料是 p 型掺杂的，器件不能完全关断，仍然有约 0.5 nA 的关电流。当栅压再次增大，高于转折点时，沟道中感应出电子，电子浓度随着栅压的进一步增大而增大，逐渐取代空穴成为多数载流子，并使源漏电流反方向逐渐增大。通过计算得出该器件的跨导为 2.268×10^{-8} S，开关比可达到 500。在栅压 V_{gs} 保持不变的条件下，源漏电压 V_{ds} 从−1 V 到 1 V 线性扫描得到器件的输出特性曲线，测试一系列 V_{gs} 值下的输出特性即可得到输出特性曲线簇，如图 4(b) 所示。可以看出，源漏电流在不同的栅压下表现出明显的分离，说明该器件具有较强的栅控能力。同时，该器件由 sc-SWCNT / C_{60} 复合薄膜在源极和漏极之间架起桥梁，全碳异质结特殊的电学和光学性质为高性能宽光谱的光电探测提供了材料基础，因此本文在室温空气中研究了器件的光电性能。图 5(a) 和 5(b) 分别展示了异质结器件在不同波长激光照射下的 I-V 曲线以及在无偏压下的 I-T 曲线。为了测试器件的光电性能，分别在 405、532、650、780、860、940、1 064 nm 波长的激光下（激光功率均为 5 mW/cm^2），使用半导体参数分析仪测试了偏置电压 V_{ds} 从−1 V 到 1 V 线性扫描下的源漏电流，可以观察到在 1 V 的偏压下，可以产生约 0.7 μA 的感应光电流。当激光反复打开和关闭时，光电流分别相应地急剧增加和减少，即该光电探测器在开关状态之间能够表现出较好的重复切换性能，器件具有较为优异的可靠性和循环稳定性。另外，该器件在 405~1 064 nm 内不同波长的激光下都有较为明显的光响应，证明了器件具有从可见光到近红外的宽光谱光电响应，并且在近红外波段显示出了一定的优势。为了进一步评价该异质结器件的光电性能，根据测试得到的光电流，分别计算了不同波长激光照射下的响应度和探测率。响应度定义为每单位面积每单位照明激光功率密度下产生的光电流，计算公式为 $R = \frac{I_p - I_d}{P \times A}$，其中 I_p 为感应光电流，I_d 为无激光照射时的暗电流，P 为光功率密度，A 为器件沟道有效区域的面积。探测率一般作为探测器探测最小光信号能力的指标，可以用来评价器件的灵敏度计算公式为 $D^* = \sqrt{\frac{A}{2qI_d}}R$，其中 q 为基本电荷，R 为响应度。计算可得，在功率密度为 5 mW/cm^2 的 940 nm 激光照射下，该器件可以达到 18.65 A/W 的响应度和 5.35×10^{11} Jones 的探测率，较好的光电响应性能源于 sc-SWCNT 超高的载流子迁移率、优异的光吸收系数、较长的激子扩散长度以及 C_{60} 对激子有效解离和转移收集。

4 结　论

利用 sc-SWCNT 独特的电子特性和高载流子迁移率，本文设计并制备了一种透明、全碳场效应晶体管型光电探测器。该场效应晶体管的组件(有源通道、源漏电极、介电层)都由碳基材料组成，可见光波段透光率均高于 80%。除了 sc-SWCNTs 提供的大吸收系数和高传导路径外，sc-SWCNT 与 C_{60} 的界面之间有适当的能带排列，光生电子-空穴对的分离也使器件的光电响应性能得到了显著提升。通过对器件进行电学测试，证明了器件具有较好的栅压控制能力，940 nm 下的响应度和探测率分别可达 18.65 A/W和 5.35×10^{11}Jones，并且可以实现 405~1 064 nm 宽光谱响应，证明了 sc-SWCNT/C_{60} 薄膜异质结用于光电探测器的巨大优势。本文所展示的结果为高性能全碳基光电器件的设计与制备提供了一个新的思路，为下一代全碳透明光电子技术的发展提供了有力的支撑。

References:

[1] Richter M, T Heumüller, Matt G J, *et al*.. Carbon photodetectors: The versatility of carbon allotropes[J]. *Advanced Energy Materials*, 2016, 7(10): 1601574.

[2] Murata T, Asahi S, Sanguinetti S, *et al*.. Infrared photodetector sensitized by InAs quantum dots embedded near an $Al_{0.3}Ga_{0.7}As$/GaAs heterointerface[J]. *Scientific Reports*, 2020, 10(1): 1-11.

[3] Xing J, Zhao K, Lu H B, *et al*.. Visible-blind, ultraviolet-sensitive photodetector based on SrTiO3 single crystal[J]. *Optics Letters*, 2007, 32(17): 2526-2528.

[4] Hirsch A. The era of carbon allotropes[J]. *Nature Materials*, 2010, 9: 868-871.

[5] Dinadayalane T C, Leszczynski J. Remarkable diversity of carbon–carbon bonds: structures and properties of fullerenes, carbon nanotubes, and graphene[J]. *Structural Chemistry*, 2010, 21(6): 1155-1169.

[6] Premkumar T, Mezzenga R, Geckeler K E. Carbon nanotubes in the liquid phase: Addressing the issue of dispersion[J]. *Small*, 2012, 8(9): 1299-1313.

[7] Cai B F, Yin H, Huo T T, *et al*.. Semiconducting single-walled carbon nanotube/graphene van der Waals junctions for highly sensitive all-carbon hybrid humidity sensors[J]. *Journal of Materials Chemistry C*, 2020, 8(10): 3386-3394.

[8] Huo T T, Yin H, Zhou D Y, *et al*.. Self-powered broadband photodetector based on single-walled carbon nanotube/GaAs heterojunctions[J]. *ACS Sustainable Chemistry & Engineering*, 2020, 8(41): 15532-15539.

[9] Ramuz M P, Vosgueritchian M, Wei P, *et al*.. Evaluation of solution-processable carbon-based electrodes for all-carbon solar cells[J]. *ACS Nano*, 2012, 6(11): 10384-10395.

[10] Baughman R H, Zakhidov A A, Heer W. Carbon nanotubes-The route toward applications[J]. *Science*, 2002, 297(5582): 787-792.

[11] Schnorr J M, Swager T M. Emerging applications of carbon nanotubes[J]. *Chemistry of Materials*, 2011, 23(3): 646-657.

[12] Chichak K S, Star A, Altoé M V P, *et al*.. Single - walled carbon nanotubes under the influence of dynamic coordination and supramolecular chemistry[J]. *Small*, 2005, 1(4): 452-461.

[13] D'Souza F, Chitta R, Sandanayaka A S D, *et al*.. Supramolecular carbon nanotube-fullerene donor-acceptor hybrids for photoinduced electron transfer[J]. *Journal of the American Chemical Society*, 2007, 129(51): 15865-15871.

[14] Long M, Wang P, Fang H, *et al*.. Progress, challenges, and opportunities for 2D material-based photodetectors[J]. *Advanced Functional Materials*, 2019, 29(19): 1803807.

[15] Zeng Q, Wang S, Yang L, *et al*.. Carbon nanotube arrays based high-performance infrared photodetector[J]. *Optical Materials Express*, 2012, 2(6): 839-848.

[16] Liu Y, Wei N, Zeng Q, *et al*.. Room temperature broadband infrared carbon nanotube photodetector with high detectivity and stability[J]. *Advanced Optical Materials*, 2016, 4(2): 238-245.

[17] Saran R, Curry R J. Solution processable 1D fullerene C_{60} crystals for visible spectrum photodetectors[J]. *Small*, 2018, 14(11): 1703624.

[18] Yin H, Zhang L, Zhu M, *et al*.. High-Performance Visible –Near-Infrared Single-Walled Carbon Nanotube

Photodetectors via Interfacial Charge-Transfer-Induced Improvement by Surface Doping[J]. *ACS Applied Materials & Interfaces*, 2022, 14(38): 43628-43636.

[19] Cheng S H, Weng T M, Lu M L, *et al*.. All carbon-based photodetectors: an eminent integration of graphite quantum dots and two-dimensional graphene[J]. *Scientific Reports*, 2013, 3(1): 1-7.

[20] Park S, Kim S J, Nam J H, *et al*.. Significant Enhancement of Infrared Photodetector Sensitivity Using a Semiconducting Single - Walled Carbon Nanotube/C_{60} Phototransistor[J]. *Advanced materials*, 2015, 27(4): 759-765.

[21] Yu X, Dong Z, Yang J K W, *et al*.. Room-temperature mid-infrared photodetector in all-carbon graphene nanoribbon-C_{60} hybrid nanostructure[J]. *Optica*, 2016, 3(9): 979-984.

[22] Zhou Z, Ding Y, Ma H, *et al*.. Bilayer nanocarbon heterojunction for full-solution processed flexible all-carbon visible photodetector[J]. *APL Materials*, 2019, 7(3): 031501.

[23] Itkis M E, Borondics F, Yu A, *et al*.. Bolometric infrared photoresponse of suspended single-walled carbon nanotube films[J]. *Science*, 2006, 312(5772): 413-416.

[24] 霍婷婷, 张冬冬, 施祥蕾, 等. 基于碳纳米薄膜/砷化镓范德华异质结的高性能自驱动光电探测器研究[J]. 中国光学, 2022, 15(2): 373.
Huo T, Zhang D, Shi X, *et al*.. High-performance self-powered photodetectors based on the carbon nanomaterial/GaAs vdW heterojunctions[J]. *Chinese Optics*, 2022, 15(2): 373. (in Chinese)

[25] Dresselhaus M S, Dresselhaus G, Saito R, *et al*.. Raman spectroscopy of carbon nanotubes[J]. *Physics Reports*, 2005, 409(2): 47-99.

[26] Farhat H, Son H, Samsonidze G G, *et al*.. Phonon softening in individual metallic carbon nanotubes due to the Kohn anomaly[J]. *Physical Review Letters*, 2007, 99(14): 145506.

[27] Das A, Sood A K, Govindaraj A, *et al*.. Doping in carbon nanotubes probed by Raman and transport measurements[J]. *Physical Review Letters*, 2007, 99(13): 136803.

[28] Hatting B, Heeg S, Ataka K, *et al*.. Fermi energy shift in deposited metallic nanotubes: A Raman scattering study[J]. *Physical Review B*, 2013, 87(16): 165442.

[29] Wroblewska A, Gordeev G, Duzynska A, *et al*.. Doping and plasmonic Raman enhancement in hybrid single walled carbon nanotubes films with embedded gold nanoparticles[J]. *Carbon*, 2021, 179: 531-540.

[30] Wang F, Dukovic G, Brus L E, *et al*.. The optical resonances in carbon nanotubes arise from excitons[J]. *Science*, 2005, 308(5723): 838-841.

[31] Maciel I O, Anderson N, Pimenta M A, *et al*.. Electron and phonon renormalization near charged defects in carbon nanotubes[J]. *Nature Materials*, 2008, 7(11): 878-883.

[32] Das A, Sood A K. Renormalization of the phonon spectrum in semiconducting single-walled carbon nanotubes studied by Raman spectroscopy[J]. *Physical Review B*, 2009, 79(23): 235429.

Author Biographics:

ZHANG Luo-xi (1997—), female, from Anyang, Henan Province, master degree, graduated from Jilin University with a bachelor degree in 2016, and obtained a master degree from Shanghai Jiaotong University in 2023, mainly engaged in the research of carbon nanotubes, optoelectronic devices and other fields. E-mail: luoxi-zhang@sjtu.edu.cn

张罗茜(1997—), 女, 河南安阳人, 硕士, 2016 年于吉林大学获得学士学位, 2023 年于上海交通大学获得硕士学位, 主要从事碳纳米管、光电子器件等领域的研究。E-mail: luoxi-zhang@sjtu.edu.cn

SU Yan-jie (1982—), male, from Shangqiu, Henan Province, Ph.D., associate researcher/doctoral supervisor, obtained his Ph.D. from Shanghai Jiaotong University in 2012, mainly engaged in the research of nanomaterials and devices. E-mail: yanjiesu@sjtu.edu.cn

苏言杰(1982—), 男, 河南商丘人, 博士, 副研究员, 博士生导师, 2012 年于上海交通大学获得博士学位, 主要从事纳米材料与器件领域的研究。E-mail: yanjiesu@sjtu.edu.cn